Fast and accurate calculation of the bootstrap current in low collisionality stellarator plasmas

Javier Escoto[1],

with J. L. Velasco[1], I. Calvo[1], M. Landreman[2] and F. I. Parra[3]

[1]Laboratorio Nacional de Fusión, CIEMAT
[2]University of Maryland
[3]Princeton Plasma Physics Laboratory

July 22, 2025

Outline

1. Introduction
2. The monoenergetic approximation to neoclassical transport
3. Block TriDiagonal (BTD) solution: the `MONKES` code
4. Neoclassical exploration of piecewise omnigenous (pwO) magnetic fields with `MONKES`
5. Conclusions

Outline

1. Introduction
2. The monoenergetic approximation to neoclassical transport
3. Block TriDiagonal (BTD) solution: the MONKES code
4. Neoclassical exploration of piecewise omnigenous (pwO) magnetic fields with MONKES
5. Conclusions

Neoclassical transport and optimization

- The Wendelstein 7-X (W7-X) experiment has proven that theory-based optimization of neoclassical transport is effective [Beidler, Nature (2021)], [Dinklage, Nature Phys. (2018)].

Neoclassical transport and optimization

- The Wendelstein 7-X (W7-X) experiment has proven that theory-based optimization of neoclassical transport is effective [Beidler, Nature (2021)], [Dinklage, Nature Phys. (2018)].
- In order to optimize stellarators, we need to be able to evaluate neoclassical properties **fast**.

Neoclassical transport and optimization

- The Wendelstein 7-X (W7-X) experiment has proven that theory-based optimization of neoclassical transport is effective [Beidler, Nature (2021)], [Dinklage, Nature Phys. (2018)].
- In order to optimize stellarators, we need to be able to evaluate neoclassical properties **fast**. The optimization of neoclassical properties has been typically addressed **indirectly** (e.g. shaping $B-$contours to close poloidally, toroidally or helically) or using **proxies**:

Neoclassical transport and optimization

- The Wendelstein 7-X (W7-X) experiment has proven that theory-based optimization of neoclassical transport is effective [Beidler, Nature (2021)], [Dinklage, Nature Phys. (2018)].
- In order to optimize stellarators, we need to be able to evaluate neoclassical properties **fast**. The optimization of neoclassical properties has been typically addressed **indirectly** (e.g. shaping $B-$contours to close poloidally, toroidally or helically) or using **proxies**:
  - ✓ Radial transport in the $1/\nu$ regime is encapsulated in ϵ_{eff} [Nemov, PoP (1999)].

Neoclassical transport and optimization

- The Wendelstein 7-X (W7-X) experiment has proven that theory-based optimization of neoclassical transport is effective [Beidler, Nature (2021)], [Dinklage, Nature Phys. (2018)].
- In order to optimize stellarators, we need to be able to evaluate neoclassical properties **fast**. The optimization of neoclassical properties has been typically addressed **indirectly** (e.g. shaping $B-$contours to close poloidally, toroidally or helically) or using **proxies**:
  - ✓ Radial transport in the $1/\nu$ regime is encapsulated in ϵ_{eff} [Nemov, PoP (1999)].
  - ✘ Analytical formulae for the parallel flow in **general** magnetic geometry are not accurate.

Neoclassical transport and optimization

- The Wendelstein 7-X (W7-X) experiment has proven that theory-based optimization of neoclassical transport is effective [Beidler, Nature (2021)], [Dinklage, Nature Phys. (2018)].
- In order to optimize stellarators, we need to be able to evaluate neoclassical properties **fast**. The optimization of neoclassical properties has been typically addressed **indirectly** (e.g. shaping $B-$contours to close poloidally, toroidally or helically) or using **proxies**:
  - ✓ Radial transport in the $1/\nu$ regime is encapsulated in ϵ_{eff} [Nemov, PoP (1999)].
  - ✘ Analytical formulae for the parallel flow in **general** magnetic geometry are not accurate.
- Codes like `KNOSOS` [Velasco, JCP (2020)] permit **direct** optimization of **radial** neoclassical transport.

Neoclassical transport and optimization

- The Wendelstein 7-X (W7-X) experiment has proven that theory-based optimization of neoclassical transport is effective [Beidler, Nature (2021)], [Dinklage, Nature Phys. (2018)].
- In order to optimize stellarators, we need to be able to evaluate neoclassical properties **fast**. The optimization of neoclassical properties has been typically addressed **indirectly** (e.g. shaping $B-$contours to close poloidally, toroidally or helically) or using **proxies**:
  - ✓ Radial transport in the $1/\nu$ regime is encapsulated in ϵ_{eff} [Nemov, PoP (1999)].
  - ✘ Analytical formulae for the parallel flow in **general** magnetic geometry are not accurate.
- Codes like `KNOSOS` [Velasco, JCP (2020)] permit **direct** optimization of **radial** neoclassical transport.
- For the two main subclasses of omnigenous fields, optimizing the bootstrap current can be important.

Neoclassical transport and optimization

- The Wendelstein 7-X (W7-X) experiment has proven that theory-based optimization of neoclassical transport is effective [Beidler, Nature (2021)], [Dinklage, Nature Phys. (2018)].
- In order to optimize stellarators, we need to be able to evaluate neoclassical properties **fast**. The optimization of neoclassical properties has been typically addressed **indirectly** (e.g. shaping $B-$contours to close poloidally, toroidally or helically) or using **proxies**:
  - ✓ Radial transport in the $1/\nu$ regime is encapsulated in ϵ_{eff} [Nemov, PoP (1999)].
  - ✘ Analytical formulae for the parallel flow in **general** magnetic geometry are not accurate.
- Codes like `KNOSOS` [Velasco, JCP (2020)] permit **direct** optimization of **radial** neoclassical transport.
- For the two main subclasses of omnigenous fields, optimizing the bootstrap current can be important.

In quasi-symmetric (QS) stellarators, the bootstrap current can be large and its effect on the magnetic configuration should be addressed during the optimization process [Landreman, PoP (2022)], [Liu, NF (2023)].

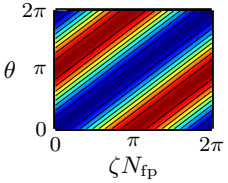

Neoclassical transport and optimization

- The Wendelstein 7-X (W7-X) experiment has proven that theory-based optimization of neoclassical transport is effective [Beidler, Nature (2021)], [Dinklage, Nature Phys. (2018)].
- In order to optimize stellarators, we need to be able to evaluate neoclassical properties **fast**. The optimization of neoclassical properties has been typically addressed **indirectly** (e.g. shaping $B-$contours to close poloidally, toroidally or helically) or using **proxies**:
  - ✓ Radial transport in the $1/\nu$ regime is encapsulated in ϵ_{eff} [Nemov, PoP (1999)].
  - ✘ Analytical formulae for the parallel flow in **general** magnetic geometry are not accurate.
- Codes like `KNOSOS` [Velasco, JCP (2020)] permit **direct** optimization of **radial** neoclassical transport.
- For the two main subclasses of omnigenous fields, optimizing the bootstrap current can be important.

Quasi-isodynamic (QI) magnetic fields (omnigenous + poloidally closed $B-$contours) **produce zero bootstrap current**. Hence, it is desirable to check that the current and/or its effect (e.g. on the island divertor) is small or minimize the current **directly**.

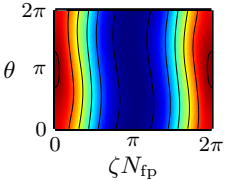

Neoclassical transport and optimization

- The Wendelstein 7-X (W7-X) experiment has proven that theory-based optimization of neoclassical transport is effective [Beidler, Nature (2021)], [Dinklage, Nature Phys. (2018)].
- In order to optimize stellarators, we need to be able to evaluate neoclassical properties **fast**. The optimization of neoclassical properties has been typically addressed **indirectly** (e.g. shaping $B-$contours to close poloidally, toroidally or helically) or using **proxies**:
  - ✓ Radial transport in the $1/\nu$ regime is encapsulated in ϵ_{eff} [Nemov, PoP (1999)].
  - ✘ Analytical formulae for the parallel flow in **general** magnetic geometry are not accurate.
- Codes like `KNOSOS` [Velasco, JCP (2020)] permit **direct** optimization of **radial** neoclassical transport.
- For the two main subclasses of omnigenous fields, optimizing the bootstrap current can be important.

Quasi-isodynamic (QI) magnetic fields (omnigenous + poloidally closed $B-$contours) **produce zero bootstrap current**. Hence, it is desirable to check that the current and/or its effect (e.g. on the island divertor) is small or minimize the current **directly**.

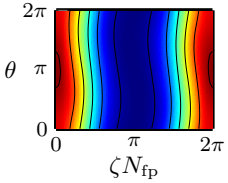

In the past, **an accurate calculation of the bootstrap current** for **general** magnetic geometry was too **slow** to include it in the optimization process.

Neoclassical transport simulations for understanding experiments

- In order to understand plasma discharges in stellarators and improve our theoretical knowledge, profile prediction simulations are crucial.

Neoclassical transport simulations for understanding experiments

- In order to understand plasma discharges in stellarators and improve our theoretical knowledge, profile prediction simulations are crucial.

- Plasma density and temperature profiles can be predicted using neoclassical transport coefficients with the `NTSS` code [Turkin, PoP (2011)].

Neoclassical transport simulations for understanding experiments

- In order to understand plasma discharges in stellarators and improve our theoretical knowledge, profile prediction simulations are crucial.

- Plasma density and temperature profiles can be predicted using neoclassical transport coefficients with the `NTSS` code [Turkin, PoP (2011)].

- Recent developments like `Trinity-GX` [Mandell, APS (2023)] or `TANGO` [Bañón, NF (2023)] combine accurate calculations of turbulent and **radial** neoclassical transport for self-consistent profile evolution.

Neoclassical transport simulations for understanding experiments

- In order to understand plasma discharges in stellarators and improve our theoretical knowledge, profile prediction simulations are crucial.

- Plasma density and temperature profiles can be predicted using neoclassical transport coefficients with the `NTSS` code [Turkin, PoP (2011)].

- Recent developments like `Trinity-GX` [Mandell, APS (2023)] or `TANGO` [Bañón, NF (2023)] combine accurate calculations of turbulent and **radial** neoclassical transport for self-consistent profile evolution.

- In the past, an accurate calculation of the bootstrap current in general magnetic geometry was too slow to be systematically included in predictive transport frameworks.

Neoclassical transport simulations for understanding experiments

- In order to understand plasma discharges in stellarators and improve our theoretical knowledge, profile prediction simulations are crucial.

- Plasma density and temperature profiles can be predicted using neoclassical transport coefficients with the `NTSS` code [Turkin, PoP (2011)].

- Recent developments like `Trinity-GX` [Mandell, APS (2023)] or `TANGO` [Bañón, NF (2023)] combine accurate calculations of turbulent and **radial** neoclassical transport for self-consistent profile evolution.

- In the past, an accurate calculation of the bootstrap current in general magnetic geometry was too slow to be systematically included in predictive transport frameworks.

The main result of my PhD is the neoclassical code `MONKES` (MONoenergetic Kinetic Equation Solver). Conceived to satisfy the necessity of **fast and accurate** calculations of the bootstrap current in stellarators.
Thus, it opens up the possibilities of **direct optimization of neoclassical transport** and to include systematically the bootstrap current effect in **predictive transport simulations**.

Outline

1. Introduction
2. The monoenergetic approximation to neoclassical transport
3. Block TriDiagonal (BTD) solution: the MONKES code
4. Neoclassical exploration of piecewise omnigenous (pwO) magnetic fields with MONKES
5. Conclusions

Monoenergetic drift-kinetic equation (DKE)

`MONKES` solves the same equation as `DKES` [Hirshman, Phys. Fluids (1986)] for the species a

$$(v\xi \boldsymbol{b} + \boldsymbol{v}_E) \cdot \nabla h_a + v \nabla \cdot \boldsymbol{b} \frac{(1-\xi^2)}{2} \frac{\partial h_a}{\partial \xi} - \nu^a \mathcal{L} h_a = S_a,$$

$$\boldsymbol{v}_E := -E_\psi(\psi) \frac{\boldsymbol{B} \times \nabla \psi}{\langle B^2 \rangle}, \qquad \mathcal{L} := \frac{1}{2} \frac{\partial}{\partial \xi} \left((1-\xi^2) \frac{\partial}{\partial \xi} \right),$$

where $\boldsymbol{b} := \boldsymbol{B}/B$, ψ is the flux surface label, $\xi := \boldsymbol{v} \cdot \boldsymbol{b}/|\boldsymbol{v}|$, $v := |\boldsymbol{v}|$, h_a is the (non-adiabatic) deviation of the distribution function from a Maxwellian and $\langle \ldots \rangle$ denotes the flux surface average.

Monoenergetic drift-kinetic equation (DKE)

`MONKES` solves the same equation as `DKES` [Hirshman, Phys. Fluids (1986)] for the species a

$$(v\xi \boldsymbol{b} + \boldsymbol{v}_E) \cdot \nabla h_a + v \nabla \cdot \boldsymbol{b} \frac{(1-\xi^2)}{2} \frac{\partial h_a}{\partial \xi} - \nu^a \mathcal{L} h_a = S_a,$$

$$\boldsymbol{v}_E := -E_\psi(\psi) \frac{\boldsymbol{B} \times \nabla \psi}{\langle B^2 \rangle}, \qquad \mathcal{L} := \frac{1}{2} \frac{\partial}{\partial \xi} \left((1-\xi^2) \frac{\partial}{\partial \xi} \right),$$

where $\boldsymbol{b} := \boldsymbol{B}/B$, ψ is the flux surface label, $\xi := \boldsymbol{v} \cdot \boldsymbol{b}/|\boldsymbol{v}|$, $v := |\boldsymbol{v}|$, h_a is the (non-adiabatic) deviation of the distribution function from a Maxwellian and $\langle \ldots \rangle$ denotes the flux surface average.

Solving the monoenergetic DKE allows to calculate, with **sufficient accuracy**, the neoclassical fluxes

$$\langle n_a \boldsymbol{V}_a \cdot \nabla \psi \rangle := \left\langle \int \boldsymbol{v}_{\mathrm{m}a} \cdot \nabla \psi \; h_a \, \mathrm{d}^3 \boldsymbol{v} \right\rangle,$$

$$\langle \boldsymbol{Q}_a \cdot \nabla \psi \rangle / T_a := \left\langle \int v^2 / v_{\mathrm{t}a}^2 \boldsymbol{v}_{\mathrm{m}a} \cdot \nabla \psi \; h_a \, \mathrm{d}^3 \boldsymbol{v} \right\rangle,$$

$$\langle n_a \boldsymbol{V}_a \cdot \boldsymbol{B} \rangle / B_0 := \left\langle B/B_0 \int v\xi \; h_a \, \mathrm{d}^3 \boldsymbol{v} \right\rangle.$$

Monoenergetic drift-kinetic equation (DKE)

The source term in the DKE is

$$S_a := f_{\mathrm{Ma}} \left[\frac{Bv^2}{\Omega_a} \left(s_1 A_{1a} + (v^2/v_{\mathrm{t}a}^2) s_2 A_{2a} \right) + v s_3 A_{3a} \right],$$

where $A_{1a}(\psi) := n_a'(\psi)/n_a(\psi) - 3T_a'(\psi)/2T_a(\psi) - e_a E_\psi(\psi)/T_a(\psi)$, $A_{2a}(\psi) := T_a'(\psi)/T_a(\psi)$, $A_{3a}(\psi) := e_a B_0(\psi) \langle \boldsymbol{E} \cdot \boldsymbol{B} \rangle / T_a(\psi) \left\langle B^2 \right\rangle$ are the thermodynamical forces and

Monoenergetic drift-kinetic equation (DKE)

The source term in the DKE is

$$S_a := f_{\mathrm{Ma}} \left[\frac{Bv^2}{\Omega_a} \left(s_1 A_{1a} + (v^2/v_{\mathrm{t}a}^2) s_2 A_{2a} \right) + v s_3 A_{3a} \right],$$

where $A_{1a}(\psi) := n_a'(\psi)/n_a(\psi) - 3T_a'(\psi)/2T_a(\psi) - e_a E_\psi(\psi)/T_a(\psi)$, $A_{2a}(\psi) := T_a'(\psi)/T_a(\psi)$, $A_{3a}(\psi) := e_a B_0(\psi) \langle \boldsymbol{E} \cdot \boldsymbol{B} \rangle / T_a(\psi) \left\langle B^2 \right\rangle$ are the thermodynamical forces and

$$s_1 := -\Omega_a B^{-1} v^{-2} \boldsymbol{v}_{\mathrm{m}a} \cdot \nabla \psi, \quad s_2 := s_1, \quad s_3 := \xi B / B_0.$$

Monoenergetic drift-kinetic equation (DKE)

The source term in the DKE is

$$S_a := f_{\mathrm{Ma}} \left[\frac{Bv^2}{\Omega_a} \left(s_1 A_{1a} + (v^2/v_{\mathrm{t}a}^2) s_2 A_{2a} \right) + v s_3 A_{3a} \right],$$

where $A_{1a}(\psi) := n_a'(\psi)/n_a(\psi) - 3T_a'(\psi)/2T_a(\psi) - e_a E_\psi(\psi)/T_a(\psi)$, $A_{2a}(\psi) := T_a'(\psi)/T_a(\psi)$, $A_{3a}(\psi) := e_a B_0(\psi) \langle \boldsymbol{E} \cdot \boldsymbol{B} \rangle / T_a(\psi) \left\langle B^2 \right\rangle$ are the thermodynamical forces and

$$s_1 := -\Omega_a B^{-1} v^{-2} \boldsymbol{v}_{\mathrm{m}a} \cdot \nabla \psi, \quad s_2 := s_1, \quad s_3 := \xi B / B_0.$$

It is convenient to use a splitting

$$h_a = f_{\mathrm{Ma}} \left[\frac{Bv}{\Omega_a} \left(A_{1a} f_1 + A_{2a} (v^2/v_{\mathrm{t}a}^2) f_2 \right) + A_{3a} f_3 \right]$$

similar to the one used in [Beidler, NF (2011)].

Monoenergetic transport coefficients

The splitting is chosen so that $\{f_j\}_{j=1}^3$ are solutions to

$$\xi \boldsymbol{b} \cdot \nabla f_j + \nabla \cdot \boldsymbol{b} \frac{(1-\xi^2)}{2} \frac{\partial f_j}{\partial \xi} - \frac{\widehat{E}_\psi}{\langle B^2 \rangle} \boldsymbol{B} \times \nabla \psi \cdot \nabla f_j - \hat{\nu} \mathcal{L} f_j = s_j,$$

for $j = 1, 2, 3$, where $\hat{\nu} := \nu(v)/v$ and $\widehat{E}_\psi := E_\psi / v$.

Monoenergetic transport coefficients

The splitting is chosen so that $\{f_j\}_{j=1}^3$ are solutions to

$$\xi \boldsymbol{b} \cdot \nabla f_j + \nabla \cdot \boldsymbol{b} \frac{(1-\xi^2)}{2} \frac{\partial f_j}{\partial \xi} - \frac{\widehat{E}_\psi}{\langle B^2 \rangle} \boldsymbol{B} \times \nabla \psi \cdot \nabla f_j - \hat{\nu} \mathcal{L} f_j = s_j,$$

for $j = 1, 2, 3$, where $\hat{\nu} := \nu(v)/v$ and $\widehat{E}_\psi := E_\psi / v$.

With each solution f_j we can compute the monoenergetic geometric coefficients

$$\widehat{D}_{ij}(\psi, v) := \left\langle \int_{-1}^{1} s_i f_j \, \mathrm{d}\xi \right\rangle, \quad i, j \in \{1, 2, 3\},$$

which for fixed $(\hat{\nu}, \widehat{E}_\psi)$ depend only on the magnetic geometry.

Monoenergetic transport coefficients

The splitting is chosen so that $\{f_j\}_{j=1}^3$ are solutions to

$$\xi \boldsymbol{b}\cdot\nabla f_j + \nabla\cdot\boldsymbol{b}\frac{(1-\xi^2)}{2}\frac{\partial f_j}{\partial \xi} - \frac{\widehat{E}_\psi}{\langle B^2\rangle}\boldsymbol{B}\times\nabla\psi\cdot\nabla f_j - \hat{\nu}\mathcal{L}f_j = s_j,$$

for $j=1,2,3$, where $\hat{\nu} := \nu(v)/v$ and $\widehat{E}_\psi := E_\psi/v$.

With each solution f_j we can compute the monoenergetic geometric coefficients

$$\widehat{D}_{ij}(\psi, v) := \left\langle \int_{-1}^{1} s_i f_j \,\mathrm{d}\xi \right\rangle, \quad i,j\in\{1,2,3\},$$

which for fixed $(\hat{\nu}, \widehat{E}_\psi)$ depend only on the magnetic geometry.

At most, four of them are independent: $\{\widehat{D}_{11}, \widehat{D}_{13}, \widehat{D}_{31}, \widehat{D}_{33}\}$. For stellarator-symmetric devices or $E_\psi = 0$ we have the Onsager relation $\widehat{D}_{13} = -\widehat{D}_{31}$.

Thermal transport coefficients

Using $\widehat{D}_{ij}$, the neoclassical fluxes can be calculated via the Onsager matrix

$$\begin{bmatrix} \langle n_a \boldsymbol{V}_a \cdot \nabla\psi \rangle \\ \langle \boldsymbol{Q}_a \cdot \nabla\psi \rangle / T_a \\ \langle n_a \boldsymbol{V}_a \cdot \boldsymbol{B} \rangle / B_0 \end{bmatrix} = \begin{bmatrix} L_{11a} & L_{12a} & L_{13a} \\ L_{21a} & L_{22a} & L_{23a} \\ L_{31a} & L_{32a} & L_{33a} \end{bmatrix} \begin{bmatrix} A_{1a} \\ A_{2a} \\ A_{3a} \end{bmatrix}.$$

Thermal transport coefficients

Using $\widehat{D}_{ij}$, the neoclassical fluxes can be calculated via the Onsager matrix

$$\begin{bmatrix} \langle n_a \boldsymbol{V}_a \cdot \nabla\psi \rangle \\ \langle \boldsymbol{Q}_a \cdot \nabla\psi \rangle / T_a \\ \langle n_a \boldsymbol{V}_a \cdot \boldsymbol{B} \rangle / B_0 \end{bmatrix} = \begin{bmatrix} L_{11a} & L_{12a} & L_{13a} \\ L_{21a} & L_{22a} & L_{23a} \\ L_{31a} & L_{32a} & L_{33a} \end{bmatrix} \begin{bmatrix} A_{1a} \\ A_{2a} \\ A_{3a} \end{bmatrix}.$$

The thermal transport coefficients L_{ija} are integrals of the monoenergetic coefficients $\widehat{D}_{ij}$

$$L_{ija} := \int_0^\infty 2\pi v^2 f_{\mathrm{M}a} w_i w_j K_{ija} \widehat{D}_{ij} \, \mathrm{d}v \,,$$

where $w_1 = w_3 = 1$, $w_2 = v^2/v_{ta}^2$ and, for each species

$$K_{ija} := -\frac{B^2 v^3}{\Omega_a^2}, \qquad i,j \in \{1,2\}; \quad K_{3ja} := \frac{B v^2}{\Omega_a}, \quad j \in \{1,2\};$$

$$K_{i3a} := -\frac{B v^2}{\Omega_a} = -K_{3ia}, \qquad i \in \{1,2\}; \quad K_{33a} := v.$$

Outline

1. Introduction
2. The monoenergetic approximation to neoclassical transport
3. Block TriDiagonal (BTD) solution: the `MONKES` code
4. Neoclassical exploration of piecewise omnigenous (pwO) magnetic fields with `MONKES`
5. Conclusions

Representation of the monoenergetic DKE in Legendre space

The solution is expanded in ξ as a truncated series of Legendre polynomials

$$f = \sum_{k=0}^{N_\xi} f^{(k)} P_k(\xi).$$

Representation of the monoenergetic DKE in Legendre space

The solution is expanded in ξ as a truncated series of Legendre polynomials

$$f = \sum_{k=0}^{N_\xi} f^{(k)} P_k(\xi).$$

In this basis the DKE is represented tridiagonally

$$L_k f^{(k-1)} + D_k f^{(k)} + U_k f^{(k+1)} = s^{(k)}, \quad k = 0, 1, \ldots N_\xi,$$

where $f^{(-1)} := 0$ and L_k, D_k, U_k are the linear differential operators

Representation of the monoenergetic DKE in Legendre space

The solution is expanded in ξ as a truncated series of Legendre polynomials

$$f = \sum_{k=0}^{N_\xi} f^{(k)} P_k(\xi).$$

In this basis the DKE is represented tridiagonally

$$L_k f^{(k-1)} + D_k f^{(k)} + U_k f^{(k+1)} = s^{(k)}, \quad k = 0, 1, \dots N_\xi,$$

where $f^{(-1)} := 0$ and L_k, D_k, U_k are the linear differential operators

$$L_k = \frac{k}{2k-1}\left(\boldsymbol{b}\cdot\nabla + \frac{k-1}{2}\boldsymbol{b}\cdot\nabla \ln B\right),$$
$$D_k = -\frac{\widehat{E}_\psi}{\langle B^2\rangle}\boldsymbol{B}\times\nabla\psi\cdot\nabla + \frac{k(k+1)}{2}\hat{\nu},$$
$$U_k = \frac{k+1}{2k+3}\left(\boldsymbol{b}\cdot\nabla - \frac{k+2}{2}\boldsymbol{b}\cdot\nabla \ln B\right).$$

Block TriDiagonal (BTD) solution: Forward elimination

Starting from $\Delta_{N_\xi} = D_{N_\xi}$ and $\sigma^{(N_\xi)} = s^{(N_\xi)}$ we obtain recursively

$$\begin{aligned} \Delta_k &= D_k - U_k \Delta_{k+1}^{-1} L_{k+1}, \\ \sigma^{(k)} &= s^{(k)} - U_k \Delta_{k+1}^{-1} \sigma^{(k+1)}. \end{aligned}$$

for $k = N_\xi - 1, N_\xi - 2, \ldots, 0$.

Block TriDiagonal (BTD) solution: Forward elimination

Starting from $\Delta_{N_\xi} = D_{N_\xi}$ and $\sigma^{(N_\xi)} = s^{(N_\xi)}$ we obtain recursively

$$\begin{aligned}\Delta_k &= D_k - U_k \Delta_{k+1}^{-1} L_{k+1},\\ \sigma^{(k)} &= s^{(k)} - U_k \Delta_{k+1}^{-1} \sigma^{(k+1)}.\end{aligned}$$

for $k = N_\xi - 1, N_\xi - 2, \ldots, 0$. Each Δ_k and $\sigma^{(k)}$ are obtained performing Gaussian elimination over

$$\left[\begin{array}{cc|c} D_k & U_k & s^{(k)} \\ L_{k+1} & \Delta_{k+1} & \sigma^{(k+1)} \end{array}\right]$$

to eliminate U_k.

Block TriDiagonal (BTD) solution: Forward elimination

Starting from $\Delta_{N_\xi} = D_{N_\xi}$ and $\sigma^{(N_\xi)} = s^{(N_\xi)}$ we obtain recursively

$$\begin{aligned}\Delta_k &= D_k - U_k \Delta_{k+1}^{-1} L_{k+1},\\ \sigma^{(k)} &= s^{(k)} - U_k \Delta_{k+1}^{-1} \sigma^{(k+1)}.\end{aligned}$$

for $k = N_\xi - 1, N_\xi - 2, \ldots, 0$. Each Δ_k and $\sigma^{(k)}$ are obtained performing Gaussian elimination over

$$\left[\begin{array}{cc|c} D_k & U_k & s^{(k)} \\ L_{k+1} & \Delta_{k+1} & \sigma^{(k+1)} \end{array}\right]$$

to eliminate U_k.

The system is factorized in a lower triangular form

$$L_k f^{(k-1)} + \Delta_k f^{(k)} = \sigma^{(k)}.$$

Block TriDiagonal (BTD) solution: Backward substitution

Now is immediate to solve the factorized equation for $f^{(k)}$

$$f^{(k)} = \Delta_k^{-1} \left(\sigma^{(k)} - L_k f^{(k-1)} \right), \quad k = 0, 1, \ldots, N_\xi,$$

to calculate $\widehat{D}_{ij} = 2 \sum_{k=0}^{2} \langle s_i^{(k)} f_j^{(k)} \rangle / (2k+1)$.

Block TriDiagonal (BTD) solution: Backward substitution

Now is immediate to solve the factorized equation for $f^{(k)}$

$$f^{(k)} = \Delta_k^{-1} \left(\sigma^{(k)} - L_k f^{(k-1)} \right), \quad k = 0, 1, \ldots, N_\xi,$$

to calculate $\widehat{D}_{ij} = 2 \sum_{k=0}^{2} \langle s_i^{(k)} f_j^{(k)} \rangle / (2k+1)$.

- Discretizing the flux-surface in $N_{\rm fs}$ points, L_k, D_k, U_k and Δ_k are approximated by square matrices of size $N_{\rm fs}$.

Block TriDiagonal (BTD) solution: Backward substitution

Now is immediate to solve the factorized equation for $f^{(k)}$

$$f^{(k)} = \Delta_k^{-1}\left(\sigma^{(k)} - L_k f^{(k-1)}\right), \quad k = 0, 1, \ldots, N_\xi,$$

to calculate $\widehat{D}_{ij} = 2\sum_{k=0}^{2}\langle s_i^{(k)} f_j^{(k)}\rangle/(2k+1)$.

- Discretizing the flux-surface in N_{fs} points, L_k, D_k, U_k and Δ_k are approximated by square matrices of size N_{fs}.

- `MONKES` employs Boozer angles (θ, ζ) and a pseudospectral Fourier discretization with N_θ and N_ζ points ($N_{\text{fs}} = N_\theta N_\zeta$). `MONKES` has spectral convergence in the three variables.

Block TriDiagonal (BTD) solution: Backward substitution

Now is immediate to solve the factorized equation for $f^{(k)}$

$$f^{(k)} = \Delta_k^{-1}\left(\sigma^{(k)} - L_k f^{(k-1)}\right), \quad k = 0, 1, \ldots, N_\xi,$$

to calculate $\widehat{D}_{ij} = 2\sum_{k=0}^{2}\langle s_i^{(k)} f_j^{(k)}\rangle/(2k+1)$.

- Discretizing the flux-surface in $N_{\rm fs}$ points, L_k, D_k, U_k and Δ_k are approximated by square matrices of size $N_{\rm fs}$.

- `MONKES` employs Boozer angles (θ, ζ) and a pseudospectral Fourier discretization with N_θ and N_ζ points ($N_{\rm fs} = N_\theta N_\zeta$). `MONKES` has spectral convergence in the three variables.

- For calculating $\widehat{D}_{ij}$ only $\{f^{(k)}\}_{k=0}^{2}$ are needed. Memory required $\sim O(N_{\rm fs}^2)$ is minimal and typically fits in a single core.

Block TriDiagonal (BTD) solution: Backward substitution

Now is immediate to solve the factorized equation for $f^{(k)}$

$$f^{(k)} = \Delta_k^{-1}\left(\sigma^{(k)} - L_k f^{(k-1)}\right), \quad k = 0, 1, \ldots, N_\xi,$$

to calculate $\widehat{D}_{ij} = 2\sum_{k=0}^{2}\langle s_i^{(k)} f_j^{(k)}\rangle/(2k+1)$.

- Discretizing the flux-surface in $N_{\rm fs}$ points, L_k, D_k, U_k and Δ_k are approximated by square matrices of size $N_{\rm fs}$.

- `MONKES` employs Boozer angles (θ, ζ) and a pseudospectral Fourier discretization with N_θ and N_ζ points ($N_{\rm fs} = N_\theta N_\zeta$). `MONKES` has spectral convergence in the three variables.

- For calculating $\widehat{D}_{ij}$ only $\{f^{(k)}\}_{k=0}^{2}$ are needed. Memory required $\sim O(N_{\rm fs}^2)$ is minimal and typically fits in a single core.

- The solution requires inverting $N_\xi + 1$ matrices of size $N_{\rm fs}$. Arithmetical complexity $\sim O(N_{\rm fs}^3 N_\xi)$ operations. Each inversion can be parallelized.

Block TriDiagonal (BTD) solution: Backward substitution

Now is immediate to solve the factorized equation for $f^{(k)}$

$$f^{(k)} = \Delta_k^{-1}\left(\sigma^{(k)} - L_k f^{(k-1)}\right), \quad k = 0, 1, \ldots, N_\xi,$$

to calculate $\widehat{D}_{ij} = 2\sum_{k=0}^{2}\langle s_i^{(k)} f_j^{(k)}\rangle/(2k+1)$.

- Discretizing the flux-surface in $N_{\rm fs}$ points, L_k, D_k, U_k and Δ_k are approximated by square matrices of size $N_{\rm fs}$.

- `MONKES` employs Boozer angles (θ, ζ) and a pseudospectral Fourier discretization with N_θ and N_ζ points ($N_{\rm fs} = N_\theta N_\zeta$). `MONKES` has spectral convergence in the three variables.

- For calculating $\widehat{D}_{ij}$ only $\{f^{(k)}\}_{k=0}^{2}$ are needed. Memory required $\sim O(N_{\rm fs}^2)$ is minimal and typically fits in a single core.

- The solution requires inverting $N_\xi + 1$ matrices of size $N_{\rm fs}$. Arithmetical complexity $\sim O(N_{\rm fs}^3 N_\xi)$ operations. Each inversion can be parallelized.

This algorithm has been implemented in the new code `MONKES` and allows an **accurate** calculation of all the $\widehat{D}_{ij}$ at (very) low collisionality in $\sim$ 1 minute on a single core. $\Rightarrow$ **`MONKES` is sufficiently fast for optimization purposes**.

Study cases for benchmarking MONKES

- At low collisionality, the solution to the DKE has internal boundary layers in ξ which makes **challenging** to solve it **fast and accurately**, specially for computing $\widehat{D}_{31}$.

Study cases for benchmarking MONKES

- At low collisionality, the solution to the DKE has internal boundary layers in ξ which makes **challenging** to solve it **fast and accurately**, specially for computing $\widehat{D}_{31}$.
- `MONKES` calculations will be benchmarked against `DKES` and `SFINCS` [Landreman, PoP (2014)].

Study cases for benchmarking MONKES

- At low collisionality, the solution to the DKE has internal boundary layers in ξ which makes **challenging** to solve it **fast and accurately**, specially for computing $\widehat{D}_{31}$.
- MONKES calculations will be benchmarked against DKES and SFINCS [Landreman, PoP (2014)].
- Three magnetic configurations are considered. Cases with $\widehat{E}_r = 0$ are in the $1/\nu$ regime (typical of electrons) and those with $\widehat{E}_r \neq 0$ in the $\sqrt{\nu}$-ν regime (typical of ions).

Configuration	$\psi/\psi_{\mathrm{lcfs}}$	$\hat{\nu}$ $[\mathrm{m}^{-1}]$	$\widehat{E}_r$ $[\mathrm{V}\cdot\mathrm{s}/\mathrm{m}^2]$
W7X-EIM	0.200	10^{-5}	0
W7X-EIM	0.200	10^{-5}	$3\cdot 10^{-4}$
W7X-KJM	0.204	10^{-5}	0
W7X-KJM	0.204	10^{-5}	$3\cdot 10^{-4}$
CIEMAT-QI4	0.250	10^{-5}	0
CIEMAT-QI4	0.250	10^{-5}	10^{-3}

Study cases for benchmarking MONKES

- At low collisionality, the solution to the DKE has internal boundary layers in ξ which makes **challenging** to solve it **fast and accurately**, specially for computing $\widehat{D}_{31}$.
- MONKES calculations will be benchmarked against DKES and SFINCS [Landreman, PoP (2014)].
- Three magnetic configurations are considered. Cases with $\widehat{E}_r = 0$ are in the $1/\nu$ regime (typical of electrons) and those with $\widehat{E}_r \neq 0$ in the $\sqrt{\nu}$-ν regime (typical of ions).

Configuration	$\psi/\psi_{\mathrm{lcfs}}$	$\hat{\nu}$ $[\mathrm{m}^{-1}]$	$\widehat{E}_r$ $[\mathrm{V}\cdot\mathrm{s}/\mathrm{m}^2]$
W7X-EIM	0.200	10^{-5}	0
W7X-EIM	0.200	10^{-5}	$3\cdot 10^{-4}$
W7X-KJM	0.204	10^{-5}	0
W7X-KJM	0.204	10^{-5}	$3\cdot 10^{-4}$
CIEMAT-QI4	0.250	10^{-5}	0
CIEMAT-QI4	0.250	10^{-5}	10^{-3}

In order to have a typical value for MONKES wall-clock time, we will select resolutions $(N_\theta, N_\zeta, N_\xi)$ for which $\widehat{D}_{31}$ at low collisionality ($\hat{\nu} = 10^{-5}$ m^{-1}) is converged up to 5−7%. This value also gives an upper bound for the wall-clock time required for computing **all the monoenergetic coefficients** $\widehat{D}_{ij}$ at higher collisionalities.

Benchmark of monoenergetic coefficients

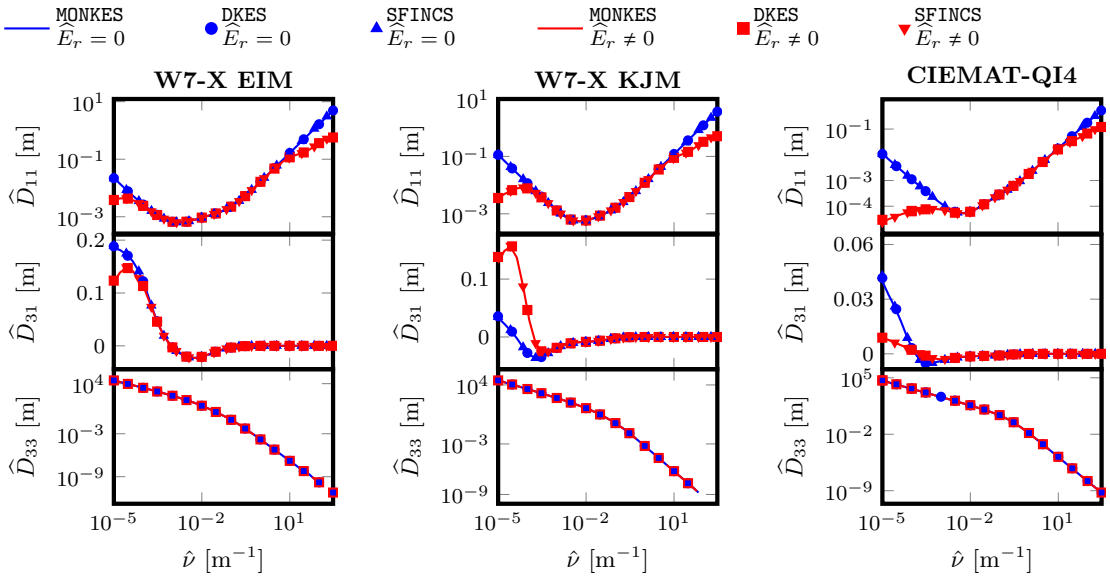

Wall-clock time for MONKES and DKES for the same level of relative convergence using a single core of CIEMAT's cluster.

Case	$t_{\text{clock}}^{\texttt{DKES}}$	$t_{\text{clock}}^{\texttt{MONKES}}$
W7X-EIM, $\widehat{E}_r = 0$	90 s	22 s
W7X-EIM, $\widehat{E}_r \neq 0$	172 s	35 s
W7X-KJM, $\widehat{E}_r = 0$	698 s	31 s
W7X-KJM, $\widehat{E}_r \neq 0$	421 s	47 s
CIEMAT-QI4, $\widehat{E}_r = 0$	1060 s	76 s
CIEMAT-QI4, $\widehat{E}_r \neq 0$	4990 s	76 s

Wall-clock time for MONKES and DKES for the same level of relative convergence using a single core of CIEMAT's cluster.

Case	$t_{\text{clock}}^{\text{DKES}}$	$t_{\text{clock}}^{\text{MONKES}}$
W7X-EIM, $\widehat{E}_r = 0$	90 s	22 s
W7X-EIM, $\widehat{E}_r \neq 0$	172 s	35 s
W7X-KJM, $\widehat{E}_r = 0$	698 s	31 s
W7X-KJM, $\widehat{E}_r \neq 0$	421 s	47 s
CIEMAT-QI4, $\widehat{E}_r = 0$	1060 s	76 s
CIEMAT-QI4, $\widehat{E}_r \neq 0$	4990 s	76 s

MONKES wall-clock time (in seconds) when running in parallel in CIEMAT's cluster.

Case \ No. cores	2	4	8	16
W7X-EIM, $\widehat{E}_r = 0$	13	8	5	5
W7X-EIM, $\widehat{E}_r \neq 0$	20	12	8	6
W7X-KJM, $\widehat{E}_r = 0$	17	12	7	7
W7X-KJM, $\widehat{E}_r \neq 0$	17	13	7	7
CIEMAT-QI4, $\widehat{E}_r = 0$	45	29	21	16
CIEMAT-QI4, $\widehat{E}_r \neq 0$	45	29	21	16

Wall-clock time for MONKES and DKES for the same level of relative convergence using a single core of CIEMAT's cluster.

Case	$t_{\text{clock}}^{\text{DKES}}$	$t_{\text{clock}}^{\text{MONKES}}$
W7X-EIM, $\widehat{E}_r = 0$	90 s	22 s
W7X-EIM, $\widehat{E}_r \neq 0$	172 s	35 s
W7X-KJM, $\widehat{E}_r = 0$	698 s	31 s
W7X-KJM, $\widehat{E}_r \neq 0$	421 s	47 s
CIEMAT-QI4, $\widehat{E}_r = 0$	1060 s	76 s
CIEMAT-QI4, $\widehat{E}_r \neq 0$	4990 s	76 s

MONKES wall-clock time (in seconds) when running in parallel in CIEMAT's cluster.

Case \ No. cores	2	4	8	16
W7X-EIM, $\widehat{E}_r = 0$	13	8	5	5
W7X-EIM, $\widehat{E}_r \neq 0$	20	12	8	6
W7X-KJM, $\widehat{E}_r = 0$	17	12	7	7
W7X-KJM, $\widehat{E}_r \neq 0$	17	13	7	7
CIEMAT-QI4, $\widehat{E}_r = 0$	45	29	21	16
CIEMAT-QI4, $\widehat{E}_r \neq 0$	45	29	21	16

MONKES is **much faster** than DKES and requires minimal memory resources. MONKES is even faster running in parallel (the CIEMAT-QI cases take 43 s on a laptop with 4 cores).

MONKES scaling

Arithmetical complexity verification: MONKES wall-clock time $\sim C_{\mathrm{alg}} N_\xi N_{\mathrm{fs}}^3$. Wall-clock times for CIEMAT's cluster cores.

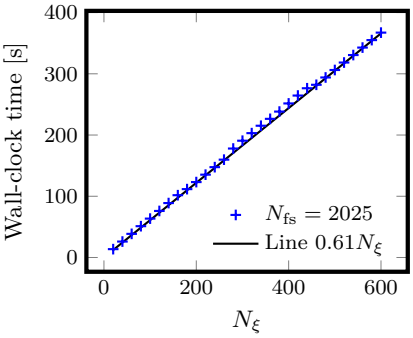

MONKES scaling

Arithmetical complexity verification: MONKES wall-clock time $\sim C_{\mathrm{alg}} N_\xi N_{\mathrm{fs}}^3$. Wall-clock times for CIEMAT's cluster cores.

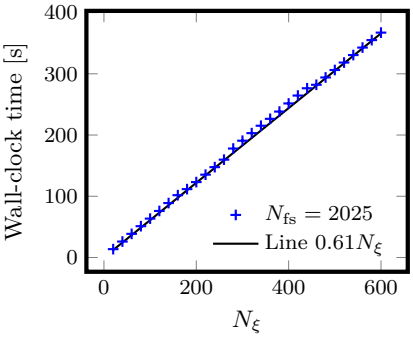

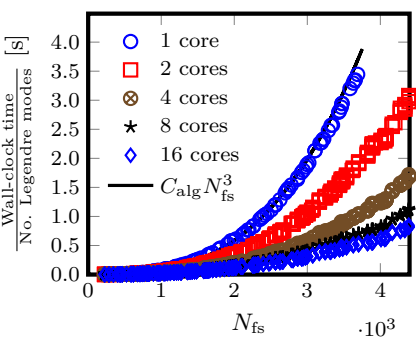

As expected, MONKES scales linearly with N_ξ and cubicly with N_{fs}. For $N_{\mathrm{fs}} \leq 2000$ and $N_\xi \leq 200$, rapid calculations (≤ 2 minutes) on a single core.

Other capabilities of MONKES: Computing derivatives of $\widehat{D}_{ij}$

Let $\eta \in \{B_{mn}, \widehat{E}_\psi, \hat{\nu}, \iota, B_\theta, B_\zeta\}$ be a parameter upon which the DKE depends.

Other capabilities of MONKES: Computing derivatives of $\widehat{D}_{ij}$

Let $\eta \in \{B_{mn}, \widehat{E}_\psi, \hat{\nu}, \iota, B_\theta, B_\zeta\}$ be a parameter upon which the DKE depends. For gradient-based optimization methods (e.g. steepest descent, Levenberg–Marquardt) it is useful to compute

$$\frac{\partial \widehat{D}_{ij}}{\partial \eta} = \left\langle \int_{-1}^{1} s_i \frac{\partial f_j}{\partial \eta} \, \mathrm{d}\xi \right\rangle + \left\langle \frac{V'}{\sqrt{g}} \int_{-1}^{1} \frac{\partial}{\partial \eta} \left(\frac{\sqrt{g} s_i}{V'} \right) f_j \, \mathrm{d}\xi \right\rangle.$$

Other capabilities of MONKES: Computing derivatives of $\widehat{D}_{ij}$

Let $\eta \in \{B_{mn}, \widehat{E}_\psi, \hat{\nu}, \iota, B_\theta, B_\zeta\}$ be a parameter upon which the DKE depends. For gradient-based optimization methods (e.g. steepest descent, Levenberg–Marquardt) it is useful to compute

$$\frac{\partial \widehat{D}_{ij}}{\partial \eta} = \left\langle \int_{-1}^{1} s_i \frac{\partial f_j}{\partial \eta} \, \mathrm{d}\xi \right\rangle + \left\langle \frac{V'}{\sqrt{g}} \int_{-1}^{1} \frac{\partial}{\partial \eta} \left(\frac{\sqrt{g} s_i}{V'} \right) f_j \, \mathrm{d}\xi \right\rangle.$$

Let f_j and g_i be, respectively, the solutions to the DKE and its **adjoint** version [Paul, JPP (2019)]

$$\textbf{DKE:} \quad \mathcal{V} f_j - \hat{\nu} \mathcal{L} f_j = s_j.$$

$$\textbf{Adjoint DKE:} \quad -\mathcal{V} g_i - \hat{\nu} \mathcal{L} g_i = s_i,$$

where $\mathcal{V} := \xi \boldsymbol{b} \cdot \nabla + \nabla \cdot \boldsymbol{b}(1-\xi^2)/2 \, \partial/\partial\xi - \widehat{E}_\psi / \langle B^2 \rangle \boldsymbol{B} \times \nabla\psi \cdot \nabla$.

Other capabilities of MONKES: Computing derivatives of $\widehat{D}_{ij}$

Let $\eta \in \{B_{mn}, \widehat{E}_\psi, \hat{\nu}, \iota, B_\theta, B_\zeta\}$ be a parameter upon which the DKE depends. For gradient-based optimization methods (e.g. steepest descent, Levenberg–Marquardt) it is useful to compute

$$\frac{\partial \widehat{D}_{ij}}{\partial \eta} = \left\langle \int_{-1}^{1} s_i \frac{\partial f_j}{\partial \eta} \,\mathrm{d}\xi \right\rangle + \left\langle \frac{V'}{\sqrt{g}} \int_{-1}^{1} \frac{\partial}{\partial \eta} \left(\frac{\sqrt{g} s_i}{V'} \right) f_j \,\mathrm{d}\xi \right\rangle.$$

Let f_j and g_i be, respectively, the solutions to the DKE and its **adjoint** version [Paul, JPP (2019)]

$$\textbf{DKE:} \quad \mathcal{V} f_j - \hat{\nu} \mathcal{L} f_j = s_j.$$
$$\textbf{Adjoint DKE:} \quad -\mathcal{V} g_i - \hat{\nu} \mathcal{L} g_i = s_i,$$

where $\mathcal{V} := \xi \boldsymbol{b} \cdot \nabla + \nabla \cdot \boldsymbol{b}(1-\xi^2)/2 \; \partial/\partial\xi - \widehat{E}_\psi / \langle B^2 \rangle \boldsymbol{B} \times \nabla\psi \cdot \nabla$.

We can compute the difficult part of $\partial \widehat{D}_{ij}/\partial\eta$ using the adjoint solution g_i as

$$\left\langle \int_{-1}^{1} s_i \frac{\partial f_j}{\partial \eta} \,\mathrm{d}\xi \right\rangle = \left\langle \int_{-1}^{1} \frac{\partial s_j}{\partial \eta} g_i \,\mathrm{d}\xi \right\rangle - \left\langle \int_{-1}^{1} g_i \mathcal{V}_\eta f_j \,\mathrm{d}\xi \right\rangle + \frac{\partial \hat{\nu}}{\partial \eta} \left\langle \int_{-1}^{1} g_i \mathcal{L} f_j \,\mathrm{d}\xi \right\rangle.$$

where $\mathcal{V}_\eta$ is the differential operator whose coefficients are the derivatives of those of $\mathcal{V}$, i.e.

$$\mathcal{V}_\eta f_j := \frac{\partial}{\partial \eta} \mathcal{V} f_j - \mathcal{V} \frac{\partial}{\partial \eta} f_j.$$

Other capabilities of MONKES: Computing derivatives of $\widehat{D}_{ij}$

An adjoint method for computing $\partial \widehat{D}_{ij}/\partial \eta$ has been implemented in MONKES.

Other capabilities of MONKES: Computing derivatives of $\widehat{D}_{ij}$

An adjoint method for computing $\partial \widehat{D}_{ij}/\partial \eta$ has been implemented in MONKES.

- The opposite of the adjoint solution $-g_i$ can be obtained as the solution to the DKE for $\hat{\nu} \mapsto -\hat{\nu}$.

Other capabilities of MONKES: Computing derivatives of $\widehat{D}_{ij}$

An adjoint method for computing $\partial \widehat{D}_{ij}/\partial \eta$ has been implemented in MONKES.

- The opposite of the adjoint solution $-g_i$ can be obtained as the solution to the DKE for $\hat{\nu} \mapsto -\hat{\nu}$.
- At the computational cost of solving twice the DKE (and some extra matrix-vector products) we can compute **all the required derivatives**.

Other capabilities of MONKES: Computing derivatives of $\widehat{D}_{ij}$

An adjoint method for computing $\partial \widehat{D}_{ij}/\partial \eta$ has been implemented in MONKES.

- The opposite of the adjoint solution $-g_i$ can be obtained as the solution to the DKE for $\hat{\nu} \mapsto -\hat{\nu}$.
- At the computational cost of solving twice the DKE (and some extra matrix-vector products) we can compute **all the required derivatives**.

Example of scan over B_{01} and B_{11} (Boozer) Fourier modes for W7-X EIM configuration at $\hat{\nu} = 10^{-5}$ m^{-1} and $\widehat{E}_r = 0$. The slope of the tangent (dashed) has been computed using MONKES.

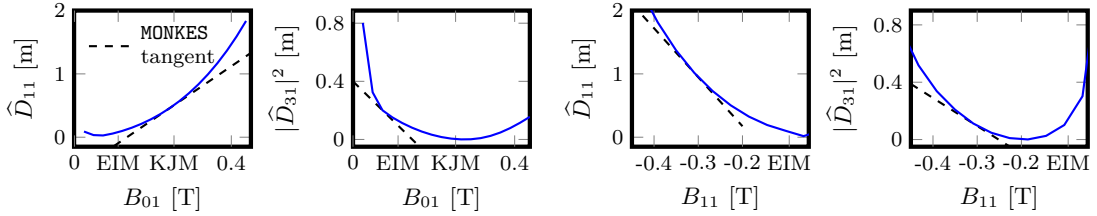

Other capabilities of MONKES: Computing derivatives of $\widehat{D}_{ij}$

An adjoint method for computing $\partial \widehat{D}_{ij}/\partial \eta$ has been implemented in MONKES.

- The opposite of the adjoint solution $-g_i$ can be obtained as the solution to the DKE for $\hat{\nu} \mapsto -\hat{\nu}$.
- At the computational cost of solving twice the DKE (and some extra matrix-vector products) we can compute **all the required derivatives**.

Example of scan over B_{01} and B_{11} (Boozer) Fourier modes for W7-X EIM configuration at $\hat{\nu} = 10^{-5}$ m^{-1} and $\widehat{E}_r = 0$. The slope of the tangent (dashed) has been computed using MONKES.

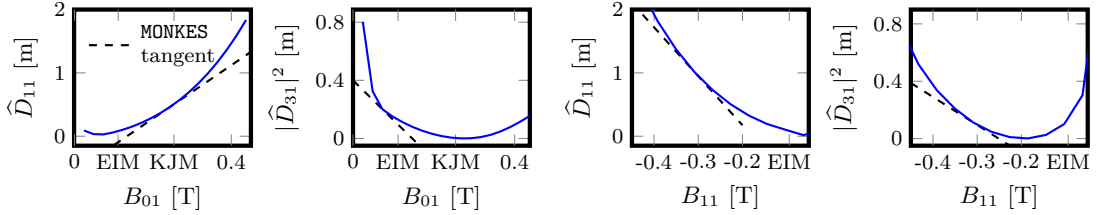

MONKES can also provide **fast and accurate** calculations of the derivatives of the monoenergetic coefficients.

Outline

1. Introduction
2. The monoenergetic approximation to neoclassical transport
3. Block TriDiagonal (BTD) solution: the MONKES code
4. Neoclassical exploration of piecewise omnigenous (pwO) magnetic fields with MONKES
5. Conclusions

Exploring piecewise omnigenous magnetic fields with MONKES

MONKES has allowed to explore the neoclassical properties of a new ideal design goal: **piecewise omnigenity** (pwO) [Velasco, PRL (2024)]. An example of pwO magnetic field is given by

$$B(\theta,\zeta) = B_{\min} + (B_{\max} - B_{\min}) \exp\left(- \left(\frac{\theta - t_\zeta \zeta}{w_\theta} \right)^{2p} - \left(\frac{\zeta - t_\theta \theta}{w_\zeta} \right)^{2p} \right),$$

$$\iota = -t_\zeta \frac{w_\zeta N_{\text{fp}}}{\pi - w_\zeta N_{\text{fp}}},$$

in the limit $p \to \infty$. As omnigenity, piecewise omnigenity implies $\epsilon_{\text{eff}} = 0$.

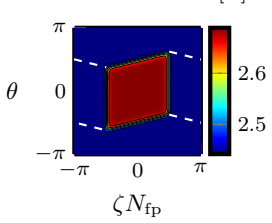

Exploring piecewise omnigenous magnetic fields with MONKES

MONKES has allowed to explore the neoclassical properties of a new ideal design goal: **piecewise omnigenity** (pwO) [Velasco, PRL (2024)]. An example of pwO magnetic field is given by

$$B(\theta,\zeta) = B_{\min} + (B_{\max} - B_{\min}) \exp\left(- \left(\frac{\theta - t_\zeta \zeta}{w_\theta} \right)^{2p} - \left(\frac{\zeta - t_\theta \theta}{w_\zeta} \right)^{2p} \right),$$

$$\iota = -t_\zeta \frac{w_\zeta N_{\mathrm{fp}}}{\pi - w_\zeta N_{\mathrm{fp}}},$$

in the limit $p \to \infty$. As omnigenity, piecewise omnigenity implies $\epsilon_{\mathrm{eff}} = 0$.

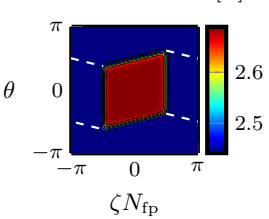

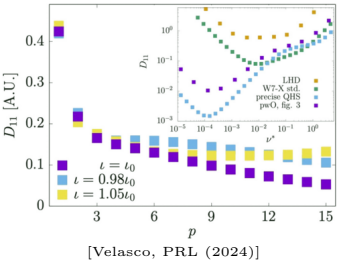

[Velasco, PRL (2024)]

- MONKES was employed to verify that proximity to pwO reduced radial transport in [Velasco, PRL (2024)].

Exploring piecewise omnigenous magnetic fields with MONKES

MONKES has allowed to explore the neoclassical properties of a new ideal design goal: **piecewise omnigenity** (pwO) [Velasco, PRL (2024)]. An example of pwO magnetic field is given by

$$B(\theta,\zeta) = B_{\min} + (B_{\max} - B_{\min}) \exp\left(- \left(\frac{\theta - t_\zeta \zeta}{w_\theta} \right)^{2p} - \left(\frac{\zeta - t_\theta \theta}{w_\zeta} \right)^{2p} \right),$$

$$\iota = -t_\zeta \frac{w_\zeta N_{\mathrm{fp}}}{\pi - w_\zeta N_{\mathrm{fp}}},$$

in the limit $p \to \infty$. As omnigenity, piecewise omnigenity implies $\epsilon_{\mathrm{eff}} = 0$.

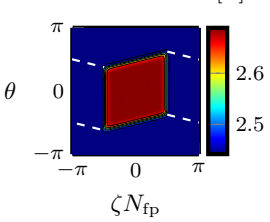

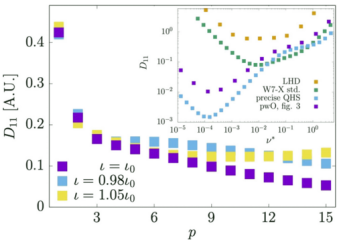

[Velasco, PRL (2024)]

- MONKES was employed to verify that proximity to pwO reduced radial transport in [Velasco, PRL (2024)].
- Very recently, in [Calvo, PRE (in press)], MONKES was employed to verify numerically that there are pwO fields with **zero bootstrap current**.

Exploring piecewise omnigenous magnetic fields with MONKES

MONKES has allowed to explore the neoclassical properties of a new ideal design goal: **piecewise omnigenity** (pwO) [Velasco, PRL (2024)]. An example of pwO magnetic field is given by

$$B(\theta,\zeta) = B_{\min} + (B_{\max} - B_{\min}) \exp\left(- \left(\frac{\theta - t_\zeta \zeta}{w_\theta} \right)^{2p} - \left(\frac{\zeta - t_\theta \theta}{w_\zeta} \right)^{2p} \right),$$

$$\iota = -t_\zeta \frac{w_\zeta N_{\mathrm{fp}}}{\pi - w_\zeta N_{\mathrm{fp}}},$$

in the limit $p \to \infty$. As omnigenity, piecewise omnigenity implies $\epsilon_{\mathrm{eff}} = 0$.

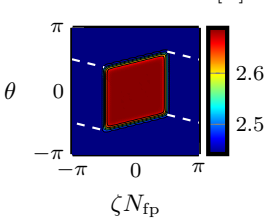

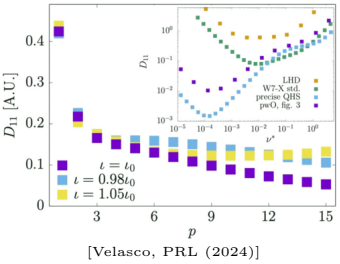
D_11 [A.U.]
p
ι = ι_0
ι = 0.98ι_0
ι = 1.05ι_0
D_11
ν*
LHD
W7-X std.
precise QHS
pwO, fig. 3

[Velasco, PRL (2024)]

- MONKES was employed to verify that proximity to pwO reduced radial transport in [Velasco, PRL (2024)].
- Very recently, in [Calvo, PRE (in press)], MONKES was employed to verify numerically that there are pwO fields with **zero bootstrap current**.

Before the findings of [Calvo, PRE (in press)], in [Escoto, NF (2025)], **deviations from QI to pwO** were explored .

Exploring piecewise omnigenous magnetic fields with MONKES: from pwO to QI

A scan in w_θ and p has been carried out to explore the impact of deviating from QI to pwO. Proximity to pwO is controlled by p and **proximity to QI** by w_θ.

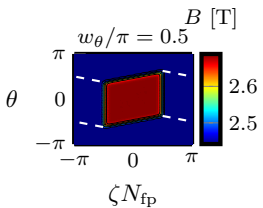

Exploring piecewise omnigenous magnetic fields with MONKES: from pwO to QI

A scan in w_θ and p has been carried out to explore the impact of deviating from QI to pwO. Proximity to pwO is controlled by p and **proximity to QI** by w_θ.

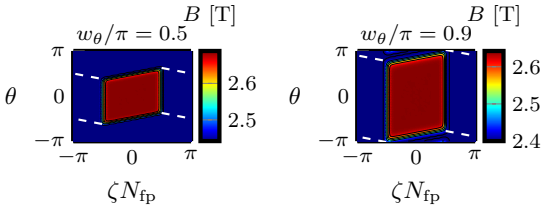

Exploring piecewise omnigenous magnetic fields with MONKES: from pwO to QI

A scan in w_θ and p has been carried out to explore the impact of deviating from QI to pwO. Proximity to pwO is controlled by p and **proximity to QI** by w_θ.

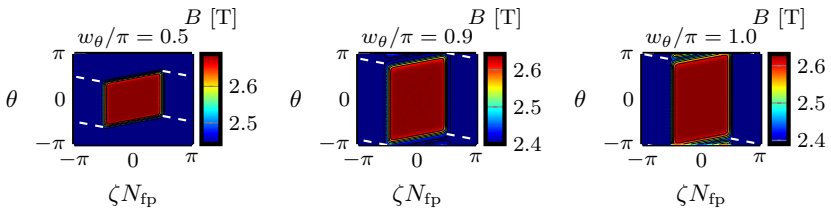

Exploring piecewise omnigenous magnetic fields with MONKES: from pwO to QI

A scan in w_θ and p has been carried out to explore the impact of deviating from QI to pwO. Proximity to pwO is controlled by p and **proximity to QI** by w_θ.

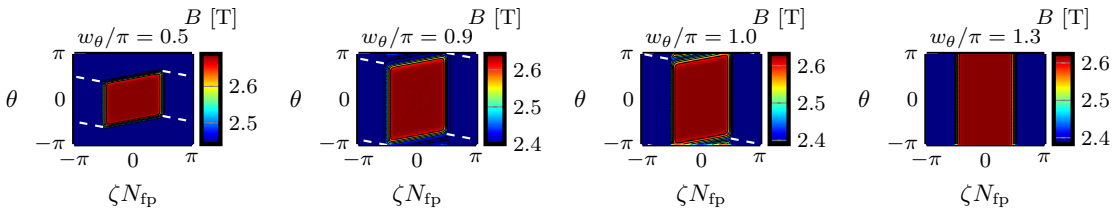

Exploring piecewise omnigenous magnetic fields with MONKES: from pwO to QI

A scan in w_θ and p has been carried out to explore the impact of deviating from QI to pwO. Proximity to pwO is controlled by p and **proximity to QI** by w_θ.

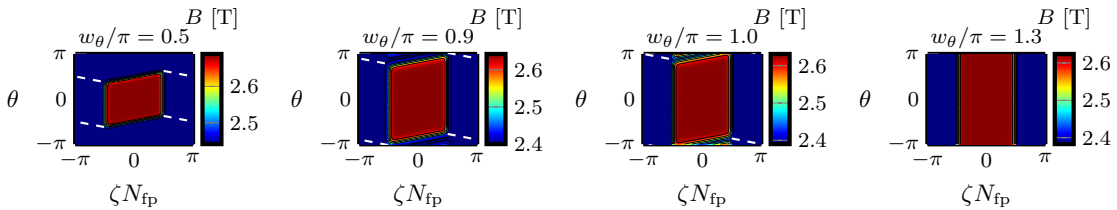

For each magnetic field, the $\widehat{D}_{11}$ and $\widehat{D}_{31}$ coefficients were evaluated using MONKES.

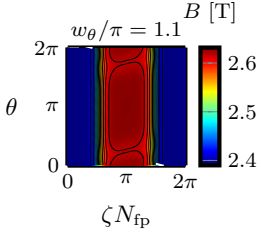

- For $p = 3$, in order to have smaller $|\widehat{D}_{31}|$ than W7X-KJM we have to be very close to QI even if some isolines of B close à la pwO.

Exploring piecewise omnigenous magnetic fields with MONKES: from pwO to QI

A scan in w_θ and p has been carried out to explore the impact of deviating from QI to pwO. Proximity to pwO is controlled by p and **proximity to QI** by w_θ.

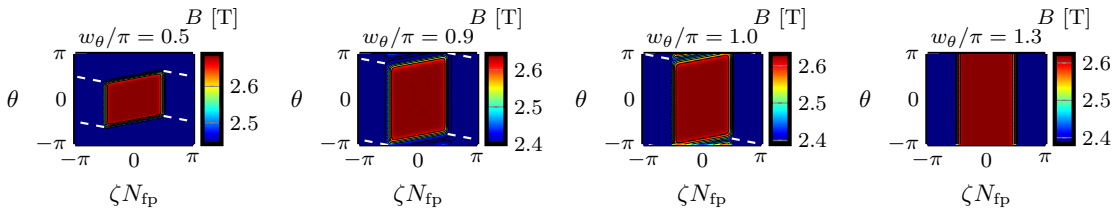

For each magnetic field, the $\widehat{D}_{11}$ and $\widehat{D}_{31}$ coefficients were evaluated using MONKES.

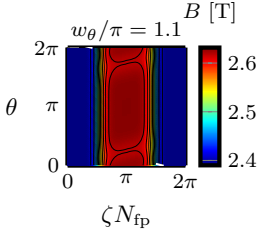

- For $p = 3$, in order to have smaller $|\widehat{D}_{31}|$ than W7X-KJM we have to be very close to QI even if some isolines of B close à la pwO.
- Solving the DKE at $\hat{\nu} = 10^{-5}$ m^{-1} for a pwO model magnetic field can require $N_{\mathrm{fs}} \sim O(10^4)$ and $N_\xi \sim 200$. This exploration **could hardly be done** without a fast neoclassical code like MONKES.

Outline

1. Introduction
2. The monoenergetic approximation to neoclassical transport
3. Block TriDiagonal (BTD) solution: the MONKES code
4. Neoclassical exploration of piecewise omnigenous (pwO) magnetic fields with MONKES
5. Conclusions

Conclusions

- `MONKES` is a new neoclassical code which is much faster than `DKES`. The code is available at `https://github.com/JavierEscoto/MONKES/`
  - `MONKES` is sufficiently fast to be included in stellarator optimization suites.

Conclusions

- `MONKES` is a new neoclassical code which is much faster than `DKES`. The code is available at `https://github.com/JavierEscoto/MONKES/`
  - `MONKES` is sufficiently fast to be included in stellarator optimization suites.
- `MONKES` is sufficiently fast to be included in predictive transport frameworks.

Conclusions

- `MONKES` is a new neoclassical code which is much faster than `DKES`. The code is available at `https://github.com/JavierEscoto/MONKES/`
  - `MONKES` is sufficiently fast to be included in stellarator optimization suites.

- `MONKES` is sufficiently fast to be included in predictive transport frameworks.
  - Opens up the possibility of treating self-consistently the bootstrap current effect in **predictive transport simulations**.

Conclusions

- `MONKES` is a new neoclassical code which is much faster than `DKES`. The code is available at `https://github.com/JavierEscoto/MONKES/`
  - `MONKES` is sufficiently fast to be included in stellarator optimization suites.
- `MONKES` is sufficiently fast to be included in predictive transport frameworks.
  - Opens up the possibility of treating self-consistently the bootstrap current effect in **predictive transport simulations**.
- `MONKES` has allowed to explore the neoclassical properties of the new family of piecewise omnigenous magnetic fields.

Conclusions

- `MONKES` is a new neoclassical code which is much faster than `DKES`. The code is available at `https://github.com/JavierEscoto/MONKES/`
  - `MONKES` is sufficiently fast to be included in stellarator optimization suites.
- `MONKES` is sufficiently fast to be included in predictive transport frameworks.
  - Opens up the possibility of treating self-consistently the bootstrap current effect in **predictive transport simulations**.
- `MONKES` has allowed to explore the neoclassical properties of the new family of piecewise omnigenous magnetic fields.
- `MONKES` quickly had an impact in the community! A JAX port of `MONKES` has been developed along with R. Conlin from the University of Maryland.

Conclusions

- `MONKES` is a new neoclassical code which is much faster than `DKES`. The code is available at `https://github.com/JavierEscoto/MONKES/`
  - `MONKES` is sufficiently fast to be included in stellarator optimization suites.
- `MONKES` is sufficiently fast to be included in predictive transport frameworks.
  - Opens up the possibility of treating self-consistently the bootstrap current effect in **predictive transport simulations**.
- `MONKES` has allowed to explore the neoclassical properties of the new family of piecewise omnigenous magnetic fields.
- `MONKES` quickly had an impact in the community! A JAX port of `MONKES` has been developed along with R. Conlin from the University of Maryland.
  - Employ `MONKES` for direct optimization within `DESC` [Dudt, PoP (2020)], [Panici, JPP (2023)], [Conlin, JPP (2023)].

Conclusions

- `MONKES` is a new neoclassical code which is much faster than `DKES`. The code is available at `https://github.com/JavierEscoto/MONKES/`
  - `MONKES` is sufficiently fast to be included in stellarator optimization suites.

- `MONKES` is sufficiently fast to be included in predictive transport frameworks.
  - Opens up the possibility of treating self-consistently the bootstrap current effect in **predictive transport simulations**.

- `MONKES` has allowed to explore the neoclassical properties of the new family of piecewise omnigenous magnetic fields.

- `MONKES` quickly had an impact in the community! A JAX port of `MONKES` has been developed along with R. Conlin from the University of Maryland.
  - Employ `MONKES` for direct optimization within `DESC` [Dudt, PoP (2020)], [Panici, JPP (2023)], [Conlin, JPP (2023)].
  - Employ `MONKES` as a preconditioner for accelerating `SFINCS` calculations.